Surface Wettability of (3-Aminopropyl)triethoxysilane Self-Assembled Monolayers

Xiangxuan Zeng, Guohua Xu,* Yuan Gao, and Yue An

Department of Chemical Engineering, Zhejiang University, Hangzhou 310027, People's Republic of China

Received: September 28, 2010; Revised Manuscript Received: November 21, 2010

The (3-aminopropyl)triethoxysilane (APTES) self-assembled monolayer (SAM) has been widely used in fundamental research and engineering applications; however, characterization of its surface wetting properties remains problematic. Surface wetting properties of the APTES SAM were systematically investigated using different contact angle measurement techniques. The observed unique nonideal wetting was related to the APTES SAM structure, including surface hydrogen bond formation, the surface roughness, and the effect of water penetration. The contact angle decreased dramatically with the residence time on the APTES SAM surface, and a special contact angle hysteresis phenomenon was observed. The contact angle could be distorted by the calculation method used for the nonideal APTES SAM surface. Values calculated by the tangent-leaning method were thought to be more accurate and credible. Our findings demonstrated that static advancing contact angles were the most stable and credible for characterizing the APTES SAM surface wettability.

1. Introduction

The (3-aminopropyl)triethoxysilane (APTES) self-assembled monolayer (SAM) has been widely used in fundamental research and engineering applications, due to its unique surface properties. Characterizing its surface wetting properties remains problematic, and reported contact angles span a wide range.[1−21] Contact angle types employed by various groups also vary considerably and include unspecified contact angles,[1,5,9,10,12−17,20] static advancing and receding contact angles,[2−4,6−8,11,19] and dynamic advancing and receding contact angles.[18,21] Currently, there remains no clear standard characterization for APTES SAM surface wetting properties.

Haller reported the first APTES SAM preparation on a silicon substrate in 1978,[1] and an advancing contact angle of 44−45° was measured using a Rame-Hart model A-100 telescope goniometer. With a self-built goniometer and sample chamber saturated with water vapor, Kurth and Bein found that advancing contact angles on the APTES SAM surface were reproducible and stable at 52 ± 2°. In contrast, receding contact angles were not reproducible.[2−4] Flink et al. performed wettability studies on the surface of the APTES SAM using a Kruss G10 contact angle measuring instrument,[11] and advancing and receding contact angles were found to be 67 ± 1° and 32 ± 1°, respectively. The large contact angle hysteresis of 35° was attributed to the absence of the highly ordered packing, arising from weak van der Waals interactions between the short propyl chains of APTES. A large contact angle hysteresis of 24° was also found by Choi and Newby, with advancing and receding contact angles of 47° and 23°, respectively (Rame-Hart model 100-00).[19] They suggested that the high contact angle hysteresis indicated the surface was rough and highly polar, and this polarity implied that APTES network formation was incomplete with many uncondensed hydroxyl or ethoxy groups. Howarter and Youngblood attempted to establish optimum reaction conditions for preparing APTES uniform thin films.[18] Dynamic contact angles (Rame-Hart advanced automated model 500 goniometer) were used to characterize surface wettability, and advancing and receding angles ranged from 51° to 93° and from 0° to 33°, respectively. The authors did not provide droplet dosing rates or advancing and receding velocities of dynamic droplets, severely limiting subsequent reproduction of their results. Similarly, Tsukruk et al. reported an advancing contact angle of 42° at a constant advancing velocity of 100 μm/s for the APTES SAM.[21]

Surface wetting properties depend strongly on the nature of the SAM. We previously prepared an APTES SAM and studied its structural features (see the Supporting Information). After about 30 min of reaction on the Si(100) substrate surface, an APTES SAM with a static advancing contact angle of 45 ± 2° and film thickness of 0.5−0.6 nm was formed from 1×10^{-3} mol/L APTES−toluene solution at 18.0 ± 0.1 °C. The C:N surface ratio estimated by X-ray photoelectron spectroscopy (XPS) indicated APTES molecules were not full hydrolyzed and that the APTES SAM was not close packed and highly organized. Atomic force microscopy (AFM) topographic analysis showed that the APTES SAM surface was rough and incompact. Theoretical molecular steric analysis of the APTES SAM structure and discussion of the SAM preparation threshold temperature indicated that it was not possible to prepare a highly organized APTES SAM under the current reaction conditions. The obtainable film was not a true SAM, rather an APTES monomolecular layer. In the current study, we have investigated the surface wetting properties of the APTES SAM in an attempt to rationalize discrepancies between reported contact angles.

2. Experimental Methods

2.1. Chemicals. APTES ($NH_2(CH_2)_3Si(OC_2H_5)_3$, 99%) was purchased from Acros Co. and used as received. Anhydrous toluene was purchased from Tedia Co. Acetone, chloroform, 2-propanol, hydrogen peroxide, hydrofluoric acid, and concentrated sulfuric acid were of analytical reagent grade. Ultrapure water with a resistivity greater than 18.2 MΩ·cm was supplied by UPWS-I-20T (Hangzhou Yongjieda Purification Technology Co. Ltd., China).

2.2. Pretreatment of Si(100) Substrates. Si(100) chips (1 cm^2) were used as substrates and were cleaned by sonication for 5 min each in acetone, chloroform, and 2-propanol. Si(100)

* To whom correspondence should be addressed. E-mail: xugh@zju.edu.cn. Phone/fax: 86-571-87951742.

10.1021/jp109259b
Published on Web 12/13/2010

chips were subsequently rinsed with excess water, sonicated for 5 min in water, and dried under a nitrogen gas stream. Cleaned substrates were then etched in hydrofluoric acid for 5 min, rinsed with water, and dried under a nitrogen gas stream. Etched substrates were oxidized in piranha solution (H_2SO_4 (98%)/H_2O_2 (30%), 70:30 (v/v)) at 90 °C for 30 min, rinsed with water, and dried under a nitrogen gas stream. A completely hydroxylated SiO_2 layer with a uniform thickness of ~2.7 nm measured by ellipsometry could then be formed on the substrate surface, such that a water contact angle of less than 4° was obtained for the final surface.

2.3. Preparation of the APTES SAM. The clean oxidized Si(100) substrate was immersed into freshly prepared 1×10^{-3} mol/L APTES−toluene at a strictly controlled temperature of 18.0 ± 0.1 °C. Following surface modification, the substrate was withdrawn as quickly as possible and immediately cleaned by sonication in toluene for 2 min, then rinsed in toluene, chloroform, and 2-propanol to remove any excess deposition, and finally dried under a nitrogen gas stream. Anhydrous toluene is hygroscopic, so the reaction was carried out in a homemade airtight vessel to exclude atmospheric humidity. Details of the preparation and characterization of the APTES SAM are available in the Supporting Information.

2.4. Contact Angle Measurements. Measurements were performed at room temperature under open-air conditions with a relative humidity of 45−50% using an OCA15plus contact angle measuring device (DataPhysics Instruments, Germany). A JY-82 contact angle measurement device equipped with a classical telescopic goniometer (Beijing Harke Experimental Instruments, China) was employed for calibration and comparison of contact angle measurements and calculations. To distinguish from the dynamic advancing/receding contact angle measured under the conditions with a continuously moving three-phase contact line, in this paper, we adopt the concept of the static advancing/receding contact angle proposed by Miyama et al.,[22] which is defined as the advancing/receding contact angle measured using the sessile droplet method.

Static contact angles were measured using the sessile droplet method. A water droplet of 2.5 μL was placed on the sample surface and an image of the droplet taken within 5 s using the charge-coupled device (CCD) video camera of the OCA15plus system. For static advancing contact angle measurement, a water droplet of 2.5 μL was added to the droplet every 30 s to allow the droplet to grow, with images captured within 5 s after addition of the droplet. This procedure was repeated nine times. For subsequent measurement of static receding contact angles, a 2.5 μL volume droplet was withdrawn from the initial 25 μL droplet every 30 s, with images captured within 5 s from removal of the droplet. This procedure was repeated until the droplet volume was less than 5.0 μL. The water droplet residence time on the sample surface was investigated to assess its effect on the contact angle. A 5 μL water droplet was placed on the sample surface, and a series of images were recorded by the CCD video camera every 20 s, until the residence time reached 10 min.

Dynamic advancing contact angle measurements were performed automatically by the OCA15plus system, using a motor-driven microsyringe to pump water steadily into the sessile drop, with the needle remaining in the drop throughout the procedure. Droplet dosing rates were 0.1, 0.5, and 1.0 μL/s, and droplet images were captured at a rate of 1 frame/s.

From the recorded images, contact angles were calculated using the tangent-leaning method available from the off-line analysis software of the OCA15plus system. All contact angle measurements were repeated at least three times for each sample, and reported values are averages of these three measurements with an error of ±2°. The contact angle formed by the first 2.5 μL water droplet on the sample surface was always found to be larger than the static advancing contact angle measured subsequently, and this angle was defined as the initial contact angle throughout this study.

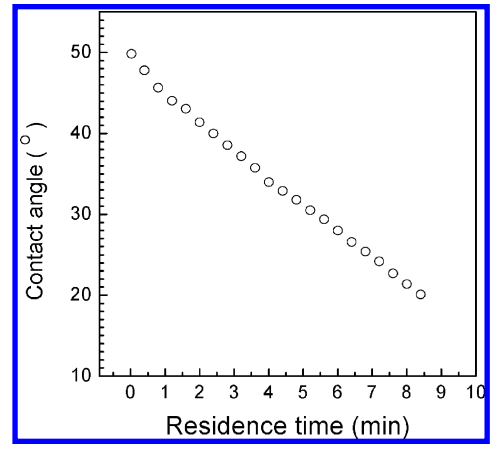

Figure 1. Change in the contact angle with increasing droplet residence time on the APTES SAM surface.

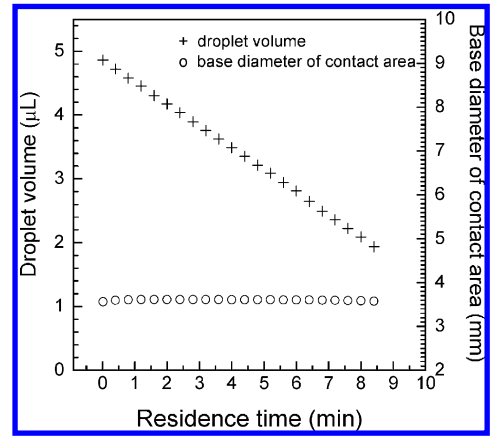

Figure 2. Change in the droplet volume and contact area with the droplet residence time.

3. Results and Discussion

3.1. Influence of the Droplet Residence Time on the Contact Angle. Figure 1 shows the change in the contact angle with the droplet residence time on the APTES SAM surface. The contact angle decreased dramatically with the residence time at a decreasing rate of ~3 deg/min. Figure 2 shows the change in the droplet volume and base diameter of the wetting area formed by the droplet on the sample surface (also called the contact area) with the residence time. Figure 2 shows that the droplet volume quickly decreased with increasing residence time, while the contact area remained constant. Since the contact angle measurement was conducted in an open-air environment, the droplet volume decrease could be attributed to evaporation. The constant contact area was unusual, in comparison to droplet behavior on an ideal solid surface.

The so-called ideal solid surface is defined as a rigid, atomically smooth, chemically homogeneous surface which is not perturbed by chemical interaction or adsorption of the liquid phase or vapor.[23] For an ideal solid surface, three surface tensions, γ_{SV}, γ_{SL}, and γ_{LV} should reside in a force balance for a stable droplet. If the droplet volume were reduced by

evaporation, this balance would be broken and a resultant force directed toward the droplet center would arise. Under this resultant force, the water droplet interface would continue to shrink until the three surface tensions achieved a new equilibrium, and finally, the contact angle would resume its original value. In summary, if the droplet volume on an ideal solid surface were reduced by evaporation, the contact angle would remain constant but the contact area would continuously shrink. In contrast, our results showed that the contact angle continuously decreased while the contact area remained constant with decreasing volume. In this situation it was impossible for the three surface tension forces to remain balanced, and this implied that additional forces existed on the three-phase contact line.

There are at least three factors which may result in additional forces, according to current knowledge of the APTES SAM. The first is surface hydrogen bonds formed between the droplet water molecules and APTES SAM surface amino groups. The second is the AFM observation which showed the APTES SAM to have a rough surface with an rms roughness of ~0.131 nm per 2 μm × 2 μm area (see the Supporting Information). The surface roughness may have caused additional surface forces to suppress shrinkage of the three-phase contact line.[24−26] Third, previous studies also revealed that the APTES SAM was not well organized and its film structure was not compact.[2−4,11,19] Menawat et al.,[27] Wei et al.,[28] and Kwok and Neumann[29] showed that water molecules can penetrate even a dense organic layer if the hydrophobic chains are too short, which may induce deformation of the organic layer. Water penetration cannot be neglected for the APTES SAM and may induce SAM deformation and result in an additional force on the sample surface.

Given the droplet was only a few microliters in volume, the influence of gravity could be ignored and the droplet shape could be treated as a spherical crown. The volume of the droplet, V, was[30]

$$V = \frac{\pi}{6}h\left(\frac{3}{4}a^2 + h^2\right) \quad (1)$$

where a is the base diameter of the contact area and h the height of the spherical crown. The value of h could be calculated as

$$h = r - \frac{a}{2\tan\theta} = \frac{a}{2\sin\theta} - \frac{a}{2\tan\theta} = \frac{a}{2\sin\theta}(1 - \cos\theta) \quad (2)$$

where r is the radius of the droplet sphere and θ the contact angle. Substituting eq 2 into eq 1 provided the relationship among the droplet volume, contact area, and contact angle, which was

$$V = \frac{\pi a^3}{48}\frac{(1 - \cos\theta)}{\sin\theta}\left[3 + \frac{(1 - \cos\theta)}{\sin^2\theta}\right] \quad (3)$$

If a remains constant at ~3.6 mm as shown in Figure 2, eq 3 provides a theoretical trend for the change in the contact angle with the droplet volume. Figure 3 shows a comparison between the experimental data and theoretical results from the spherical crown model. With the exception of the initial several data points, the spherical crown model fitted the experimental data very well, which demonstrated our conjecture is reasonable.

When a droplet contacts a "virgin" surface for the first time, a short period of time may be needed to obtain equilibrium between the droplet and surface. The system was initially in a metastable state, which may have accounted for deviation of the model from the initial data points.

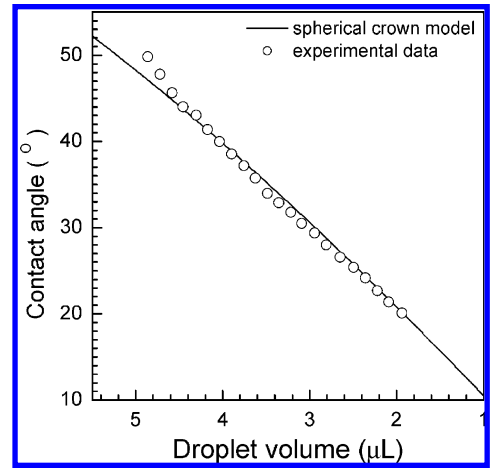

Figure 3. Trend of the contact angle with the droplet volume, showing a comparison of experimental data and theoretical results from the spherical crown model.

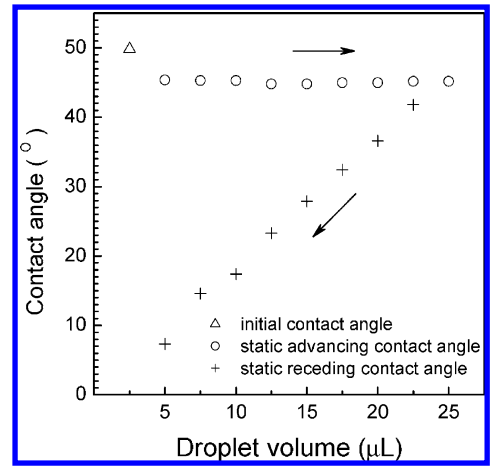

Figure 4. Change in the static advancing and receding contact angles with the droplet volume.

3.2. APTES SAM Surface Contact Angle Hysteresis. Figure 4 shows the static advancing and receding contact angle measurement processes in detail. We have shown that the APTES SAM behaved as a unique nonideal surface and a special contact angle hysteresis phenomenon was observed, which to the best of our knowledge has not been previously reported. Figure 4 shows that, with increasing droplet volume, static advancing contact angles were stable and reproducible at ~45° but static receding contact angles decreased dramatically with decreasing droplet volume. Upon a decrease of the droplet volume from 25 to 5 μL, the static receding contact angle decreased from 45° to less than 10° while the contact area remained constant (Figure 5). This process was analogous to the change in the contact angle with the residence time, with the exception of the droplet volume reduced evaporatively and artificially in the former and latter processes, respectively. Since the three-phase contact line did not recede with decreasing volume, the measured contact angles could not strictly be called receding contact angles. However, to remain consistent with common usage, we will still refer to the above angles as receding contact angles.

It was interesting to find that the contact angle formed from the first droplet on the surface (defined as the initial contact angle in this study) was always ~5° larger than subsequently

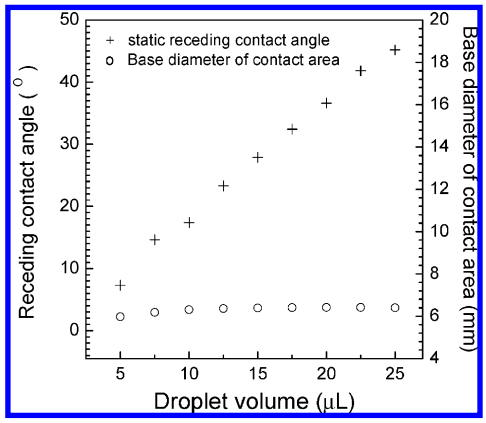

Figure 5. Change in the static receding contact angle and base diameter of the contact area with the droplet volume.

measured static advancing contact angles (Figure 4). We attributed this phenomenon to the formation of a precursor film on the sample surface.[31] The initial contact angle was formed on the APTES SAM surface while it was in a relatively dry state. After penetration from the droplet, water would wet the local film somewhat and then spread over the surface to form the so-called precursor film (thus making the surrounding originally dry surface somewhat wet). When subsequent droplets were added and spread over the surface, they were actually spread over an already wetted film surface which was more hydrophilic than the virgin surface, thus resulting in the contact angle decrease.

3.3. Contact Angle Calculation Methods. ***3.3.1. Contact Angle Fitting Method for Nonideal Surfaces.*** All contact angle measurements in this study were performed on an OCA15plus contact angle measuring device. This system offers four analysis methods for contact angle calculation, including circle-fitting, ellipse-fitting, Laplace−Young fitting, and tangent-leaning methods. The circle-fitting method finds the theoretical circle curve which best matches the droplet profile extracted from the droplet image, from which the contact angle is calculated by the numerical integration of the fitting circle curve at the three-phase contact point. The circle-fitting method is relatively accurate for small droplets where gravity can be ignored. Similarly, the ellipse-fitting method fits the drop profile as a part of an elliptical curve, and the contact angle is calculated by the numerical integration of the curve at the three-phase contact point. This method takes into account the influence of gravity on the drop shape and is more reliable for larger drops. The Laplace−Young fitting method fits the droplet profile to the Laplace−Young equation and is much more reliable when the contact angle is larger than 60°. The strategy employed in the above three methods is to fit the shape of the real drop to a theoretical drop profile according to the equation of a circle, ellipse, or Laplace−Young model. These methods find the theoretical profile that best matches the drop profile, from which the contact angle is calculated by numerical computing.[32] Experimental drops are assumed to be axisymmetric; particularly the local profile near the three-phase contact line is assumed to be representative of the bulk profile of the droplet. In theory, only a droplet on an ideal surface could satisfy these conditions.[31,32] The tangent-leaning method determines the contact angle by directly making a tangent at the three-phase contact point and measuring the contact angle using a goniometer. Only the local profile very near the three-phase contact point is taken into consideration; therefore, this method can be applied to any situation, whether the droplet profile is axisymmetric or not. The local profile near the three-phase contact point

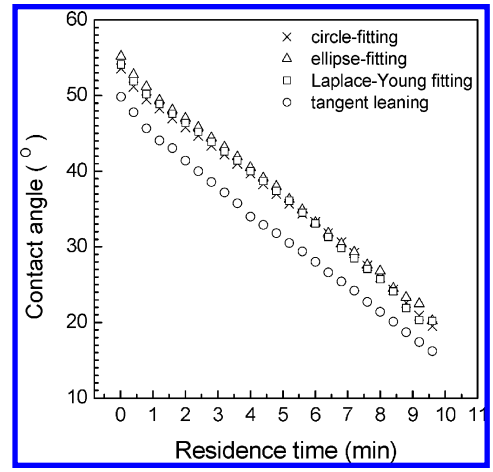

Figure 6. Change in the contact angle with the residence time, obtained from four different calculation methods.

for a droplet on a nonideal surface is generally not consistent with the bulk profile.[31,32] Thus, the contact angle calculated by the tangent-leaning method is considered more credible and accurate, as it reflects the true wetting properties of the surface.

Figure 6 shows the change in the contact angle with the droplet residence time, obtained using the four different calculation methods. Contact angles calculated by the circle-fitting, ellipse-fitting, and Laplace−Young fitting methods were remarkably similar and were ∼6° higher than those obtained from the tangent-leaning method. Contact angles calculated by the tangent-leaning method were demonstrated to be identical to those directly measured with a classical telescopic goniometer from a JY-82 contact angle measurement device. Due to influences from surface hydrogen bonding, surface roughness, and water penetration effects, the local droplet profile on the three-phase contact line may have deviated from the profile of the bulk droplet. Thus, the authenticity of contact angles calculated from the first three fitting methods is questionable.

Regrettably, in most previous studies reporting contact angles, the authors failed to specify their calculation method, which may have resulted in discrepancies between reported values. In light of our results, the tangent-leaning method is more credible and accurate for the characterization of contact angles on nonideal surfaces such as APTES SAMs.

3.3.2. Dynamic Advancing Contact Angle for Nonideal Surfaces. Dynamic contact angles have also been used to characterize the surface wetting of APTES SAMs.[18,21] Dynamic advancing contact angles were found to be strongly influenced by the advance rate of the droplet. Figure 7 shows that a dynamic advancing contact angle of ∼56° was maintained when the droplet dosing rate was 0.1 μL/s. Increasing the rate to 0.5 and 1.0 μL/s resulted in the dynamic advancing contact angles increasing to ∼60° and ∼68°, respectively. In contrast, the static advancing contact angle was constant and stable with increasing volume, which was more suitable for the characterization of the APTES SAM surface wettability.

4. Conclusions

(1) The APTES SAM displayed unique nonideal surface wetting. The contact angle decreased dramatically with the droplet residence time, with a decreasing rate of ∼3 deg/min. A special contact angle hysteresis phenomenon was observed, and static advancing contact angles were stable and reproducible at ∼45°. The static receding contact angle dropped dramatically with decreasing droplet volume.

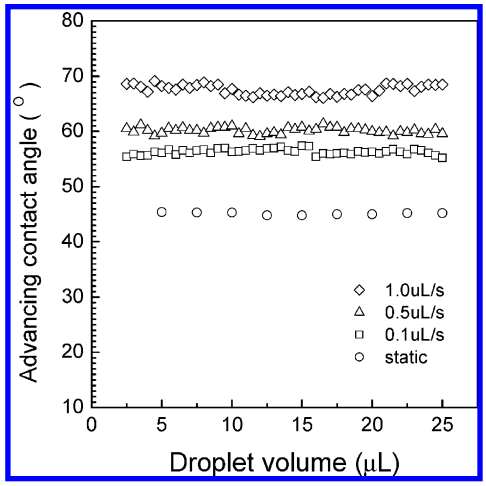

Figure 7. Static and dynamic advancing contact angles for different droplet dosing rates.

(2) The observed unique nonideal wetting was related to the APTES SAM structure, including surface hydrogen bond formation, the surface roughness, and the effect of water penetration.

(3) The contact angle value was dependent on the calculation method. For the characterization of wetting on a nonideal surface such as an APTES SAM, the tangent-leaning method was more credible and accurate, which reflected the real wetting property of the film surface.

(4) The static advancing contact angle was stable and reproducible at ~45° and was much more stable and credible than other contact angle measurement types for the characterization of the APTES SAM surface wetting.

Acknowledgment. We thank Dr. Wenge Jiang, Prof. Haihua Pan, and Prof. Ruikang Tang of the Department of Chemistry and Center for Biomaterials and Biopathways at Zhejiang University for their experimental assistance and helpful discussions. This work was supported by the National Natural Science Foundation of China (Grants 20276057 and 20701032).

Supporting Information Available: Details of the preparation and characterization of the APTES SAM. This material is available free of charge via the Internet at http://pubs.acs.org.

References and Notes

(1) Haller, I. *J. Am. Chem. Soc.* **1978**, *100*, 8050–8055.
(2) Kurth, D. G.; Bein, T. *Angew. Chem., Int. Ed. Engl.* **1992**, *31*, 336–338.
(3) Kurth, D. G.; Bein, T. *Langmuir* **1993**, *9*, 2965–2973.
(4) Kurth, D. G.; Bein, T. *Langmuir* **1995**, *11*, 3061–3067.
(5) Kowalczyk, D.; Slomkowski, S.; Chehimi, M. M.; Delamar, M. *Int. J. Adhes. Adhes.* **1996**, *16*, 227–232.
(6) Chang, Y.-Ch.; Frank, C. *Langmuir* **1996**, *12*, 5824–5829.
(7) Chang, Y.-Ch.; Frank, C. W. *Langmuir* **1998**, *14*, 326–324.
(8) Petri, D. F. S.; Wenz, G.; Schunk, P.; Schimmel, T. *Langmuir* **1999**, *15*, 4520–4523.
(9) Wei, Z. Q.; Wang, C.; Zhu, C. F.; Zhou, C. Q.; Xu, B.; Bai, C. L. *Surf. Sci.* **2000**, *459*, 401–412.
(10) Heiney, P. A.; Grüneberg, K.; Fang, J. *Langmuir* **2000**, *16*, 2651–2657.
(11) Flink, S.; van Veggel, F. C. J. M.; Reinhoudt, D. N. *J. Phys. Org. Chem.* **2001**, *14*, 407–415.
(12) Jain, S. C.; Tanwar, V. K.; Dixit, V.; Verma, S. P.; Samanta, S. B. *Appl. Surf. Sci.* **2001**, *182*, 350–356.
(13) Simon, A.; Cohen-Bouhacina, T.; Porté, M. C.; Aimé, J. P.; Baquey, C. *J. Colloid Interface Sci.* **2002**, *251*, 278–283.
(14) Ren, S.; Yang, S.; Zhao, Y. *Langmuir* **2003**, *19*, 2763–2767.
(15) Kim, J.-K.; Shin, D.-S.; Chung, W.-J.; Jang, K.-H.; Lee, K.-N.; Kim, Y.-K.; Lee, Y.-S. *Colloids Surf. B* **2004**, *33*, 67–75.
(16) Park, J.; Lee, H. *Mater. Sci. Eng., C* **2004**, *24*, 311–314.
(17) Osaki, T.; Zimmermann, R.; Kratzmüller, T.; Schweiss, R.; Werner, C. *Langmuir* **2004**, *20*, 524–527.
(18) Howarter, J. A.; Youngblood, J. P. *Langmuir* **2006**, *22*, 11142–11147.
(19) Choi, S.-H.; Newby, B.-m. Z. *Surf. Sci.* **2006**, *600*, 1391–1404.
(20) Qin, M.; Hou, S.; Wang, L.; Feng, X.; Wang, R.; Yang, Y.; Wang, C.; Yu, L.; Shao, B.; Qiao, M. *Colloids Surf., B* **2007**, *60*, 243–249.
(21) Tsukruk, V. V.; Bliznyuk, V. N.; Visser, D.; Campbell, A. L.; Bunning, T. J.; Adams, W. W. *Macromolecules* **1997**, *30*, 6615–6625.
(22) Miyama, M.; Yang, Y.; Yasuda, T.; Okuno, T.; Yasuda, H. K. *Langmuir* **1997**, *13*, 5494–5503.
(23) Good, R. J. *J. Adhes. Sci. Technol.* **1992**, *6*, 1269–1302.
(24) Israelachvili, J. *Intermolecular and Surface Forces*, 2nd ed.; Academic Press: London, 1992; Chapter 15.
(25) Blake, T. D.; Haynes, J. M. *J. Colloid Interface Sci.* **1969**, *30*, 421.
(26) Semal, S.; Blake, T. D.; Geskin, V.; de Ruijter, M. J.; Castelein, G.; De Coninck, J. *Langmuir* **1999**, *15*, 8765–8770.
(27) Menawat, A.; Henry, J.; Siriwardane, R. *J. Colloid Interface Sci.* **1984**, *101*, 110–119.
(28) Wei, M.; Bowman, R. S.; Wilson, J. L.; Morrow, N. R. *J. Colloid Interface Sci.* **1992**, *157*, 154–159.
(29) Kwok, D. Y.; Neumann, A. W. *Ad. Colloid Interface Sci.* **1999**, *81*, 167–249.
(30) Beyer, W. H. *CRC Standard Mathematical Tables*, 26th ed.; CRC Press: Boca Raton, FL, 1981; Chapter 4.
(31) Good, R. J.; Koo, M. N. *J. Colloid Interface Sci.* **1979**, *72*, 283–292.
(32) Kwok, D. Y.; Leung, A.; Lam, C. N. C.; Li, A.; Wu, R.; Neumann, A. W. *J. Colloid Interface Sci.* **1998**, *206*, 44–51.

JP109259B